SEMARAK ILMU PUBLISHING

Journal of Advanced Research in Applied Sciences and Engineering Technology

Journal homepage:
https://semarakilmu.com.my/journals/index.php/applied_sciences_eng_tech/index
ISSN: 2462-1943



Fe_3O_4/BiOI Heterojunction Photocatalyst for Enhanced Visible Light Degradation and Detoxification of Rhodamine B Dye

Nur Lina Syahirah Mustapa[1], Mohamed Syazwan Osman[1,*], Anis Syuhada Saufi[1], Noor Fitrah Abu Bakar[2,3], Uraiwan Sirimahachai[4]

[1] EMZI-UiTM Nanoparticles Colloids and Interface Industrial Research Laboratory (NANO-CORE), Faculty Chemical Engineering, Universiti Teknologi MARA, Cawangan Pulau Pinang, 13500, Permatang Pauh, Pulau Pinang, Malaysia
[2] Faculty Chemical Engineering, Universiti Teknologi MARA, 40450, Shah Alam, Selangor, Malaysia
[3] Institute of Science, Universiti Teknologi MARA, 40450, Shah Alam, Malaysia
[4] Center of Excellence for Innovation in Chemistry, Division of Physical Science, Faculty of Science, Prince of Songkla University, Hat Yai, 90110, Songkhla, Thailand

ARTICLE INFO

Article history:
Received 3 September 2026
Received in revised form 15 September 2026
Accepted 18 September 2026
Available online 28 September 2026

Keywords:
Heterojunction; Magnetic; Photocatalyst; Rhodamine B; Toxicity

ABSTRACT

Synthetic dye such as Rhodamine B poses a serious risk to aquatic ecosystems and human health. In this work, a magnetically recoverable Fe_3O_4/BiOI heterojunction was synthesized via an in-situ precipitation route. The physicochemical properties of BiOI, Fe_3O_4, and the Fe_3O_4/BiOI composite were characterized by zeta potential and dynamic light scattering (DLS). The smaller particle size and lower polydispersity index of the composite relative to bare Fe_3O_4 indicate reduced agglomeration upon BiOI deposition. UV-Vis diffuse reflectance analysis showed that the band gap narrowed from 1.77 eV for BiOI to 1.08 eV for the Fe_3O_4/BiOI composite, indicating enhanced visible light harvesting after heterojunction formation. The photocatalytic performance was evaluated through the degradation of RhB under visible light irradiation. The Fe_3O_4/BiOI composite achieved approximately 79% RhB removal within 60 minutes of visible light exposure, considerably higher than BiOI (20%) and Fe_3O_4 (31%) alone, and the degradation followed pseudo-first-order kinetics with a rate constant of 0.0232 min^{-1}. A garden cress germination bioassay further confirmed that the treated solution was substantially less phytotoxic than the untreated dye solution, with seedling growth recovering close to the tap water control. These findings support Fe_3O_4/BiOI as a promising, magnetically separable photocatalyst for the visible-light-driven remediation of dye-contaminated water.

1. Introduction

The discharge of synthetic dyes from textile, leather, paper, and cosmetic industries has become one of the most visible forms of water pollution worldwide. Rhodamine B (RhB), a cationic xanthene dye widely used as a colourant, is of particular concern because it is chemically stable, poorly biodegradable, and reported to be carcinogenic and neurotoxic, so its presence in surface water and groundwater threatens aquatic organisms and, indirectly, human health through the food chain [1], [2]. Conventional treatment methods, such as coagulation-flocculation, adsorption, ion exchange,

* *Corresponding author.*
E-mail address: syazwan.osman@uitm.edu.my

membrane filtration, and biological treatment, generally transfer the dye from one phase to another rather than destroying it, and often leave behind concentrated sludge that requires further disposal [3]. Advanced oxidation processes (AOPs) address this limitation by generating highly reactive oxygen species that mineralise organic pollutants into carbon dioxide, water, and simple inorganic ions, and semiconductor photocatalysis has become one of the most actively researched AOPs because it can be driven by sunlight and operated at ambient temperature and pressure [4]. For example, titanium dioxide (TiO_2), zinc oxide (ZnO), graphitic carbon nitride (g-C_3N_4), and bismuth oxyhalides (BiOX) have all been investigated as semiconductor photocatalysts for visible-light-driven dye degradation [24].

Among the bismuth oxyhalides, Bismuth Oxyiodide (BiOI) has attracted particular attention because its narrow band gap of around 1.8 eV allows strong visible light absorption, and its layered $[Bi_2O_2]^{2+}$ structure generates an internal polarisation field that assists charge separation [5]. However, BiOI alone still suffers from rapid recombination of photogenerated electron-hole pairs, tends to agglomerate in suspension, and is difficult to recover after treatment, all of which limit its practical reuse. Coupling BiOI with a second semiconductor to form a heterojunction has therefore become a common strategy to improve charge separation and extend photocatalytic activity. For instance, recent studies have reported BiOI/Bi_2O_3/MgO [6], Co_3O_4/BiOBr/BiOI [7], $BiOIO_3$/$Bi_{12}O_{17}Cl_2$ [8], g-C_3N_4/BiOI [9], and ZnO/BiOI/AgI heterojunctions [10], each showing markedly higher Rhodamine B removal than bare BiOI as a result of improved interfacial charge transfer.

A complementary strategy is to couple the photocatalyst with magnetic iron oxide (Fe_3O_4) nanoparticles, which allows the spent catalyst to be recovered from treated water with a simple magnet rather than by filtration or centrifugation, an important consideration for scale-up. Fe_3O_4 itself possesses a narrow band gap and can participate in interfacial charge transfer and Fenton-like radical generation, further suppressing electron-hole recombination when combined with a visible-light-active semiconductor[24]. For instance, among the still-limited number of magnetically coupled bismuth oxyhalide systems reported, Fe_3O_4/BiOCl [11] and Fe_3O_4/TiO_2 [12] heterostructures both retained high Rhodamine B removal efficiency over repeated cycles owing to their magnetic recoverability, while standalone Fe_3O_4 nanoparticles have also shown intrinsic, if modest, photocatalytic activity towards several dyes [13].

Despite this progress, relatively few studies combine an in-situ synthesized Fe_3O_4/BiOI heterojunction with a systematic assessment of the composite's colloidal stability and, more importantly, with direct ecotoxicological verification that photocatalytic treatment actually detoxifies the effluent rather than merely decolourising it. Seed germination bioassays have recently been used to confirm genuine detoxification following photocatalytic dye treatment [13], [14], [15], and this approach is adopted here. The present study therefore synthesises Fe_3O_4/BiOI via an in-situ precipitation route, characterises the resulting composite by zeta potential and dynamic light scattering, evaluates its photocatalytic performance towards RhB degradation under visible light, and assesses the phytotoxicity of the treated solution using a garden cress seeds germination assay.

2. Methodology

2.1 Materials

Iron(II) sulfate heptahydrate ($FeSO_4 \cdot 7H_2O$), iron(III) chloride hexahydrate ($FeCl_3 \cdot 6H_2O$), ammonium hydroxide (NH_4OH), bismuth(III) nitrate pentahydrate ($Bi(NO_3)_3 \cdot 5H_2O$), potassium iodide (KI), ethylene glycol (EG), ethanol, and deionized water were used for the synthesis of Fe_3O_4, BiOI, and Fe_3O_4/BiOI composites. Rhodamine B (RhB), and hydrogen peroxide (H_2O_2) were used for the synthesis and photocatalytic experiments. All chemicals were of analytical grade and purchased from Sigma-Aldrich (Merck, USA). All chemicals were of analytical grade and used as received without

further purification. Garden cress (Lepidium sativum) seeds and commercial tap water were used for the phytotoxicity assessment.

2.2 Synthesis of Fe_3O_4

Fe_3O_4 nanoparticles were synthesized via the chemical co-precipitation method, as previously reported [16]. Briefly, aqueous solutions of $FeSO_4 \cdot 7H_2O$ and $FeCl_3 \cdot 6H_2O$ were prepared at a Fe^{2+}:Fe^{3+} molar ratio of 1:2 and mixed under continuous stirring. The reaction was conducted under a nitrogen (N_2) atmosphere to minimize the oxidation of Fe^{2+} ions. Subsequently, 20 mL of NH_4OH was added dropwise to the mixed precursor solution under continuous stirring until an alkaline pH was attained, resulting in the formation of a black Fe_3O_4 precipitate. The precipitate was magnetically separated and washed repeatedly with deionized water and ethanol until a neutral pH was obtained. The resulting Fe_3O_4 nanoparticles were then dried at 60 °C for 6 h.

2.3 Synthesis of BiOI

BiOI was synthesized via an in-situ precipitation route using EG as the reaction medium. Briefly, 0.5 mmol of $Bi(NO_3)_3 \cdot 5H_2O$ was dissolved in 35 mL of EG under vigorous stirring until a homogeneous precursor solution was obtained. Subsequently, 0.5 mmol of KI was added dropwise to the bismuth precursor solution under continuous stirring. The addition of KI resulted in the immediate formation of BiOI, as indicated by the development of a dark orange-brown suspension. Stirring was continued to facilitate the completion of the precipitation reaction. The resulting BiOI precipitate was collected by centrifugation at 4000 rpm for 10 min, followed by repeated washing with deionized water and ethanol to remove residual ions and unreacted precursors. The purified product was dried at 60 °C for 12 h to obtain BiOI powder.

2.4 Synthesis of Fe_3O_4/BiOI

The Fe_3O_4/BiOI heterojunction was synthesized by in-situ precipitation of BiOI in the presence of pre-synthesized Fe_3O_4 nanoparticles, as illustrated in Figure 1. Briefly, Fe_3O_4 nanoparticles were first dispersed in an EG solution containing $Bi(NO_3)_3 \cdot 5H_2O$ under continuous stirring to promote interaction between the Fe_3O_4 surface and the bismuth precursor. Subsequently, KI was added dropwise to the suspension under continuous stirring, inducing the in-situ formation of BiOI on the Fe_3O_4 surface. The amounts of Fe_3O_4 and BiOI precursors were adjusted to obtain a 1:1 Fe_3O_4:BiOI mass ratio. The resulting Fe_3O_4/BiOI composite was magnetically separated, washed repeatedly with deionized water and ethanol, and dried at 60 °C for 12 h. The obtained powder was subsequently used for further characterization and photocatalytic experiments.

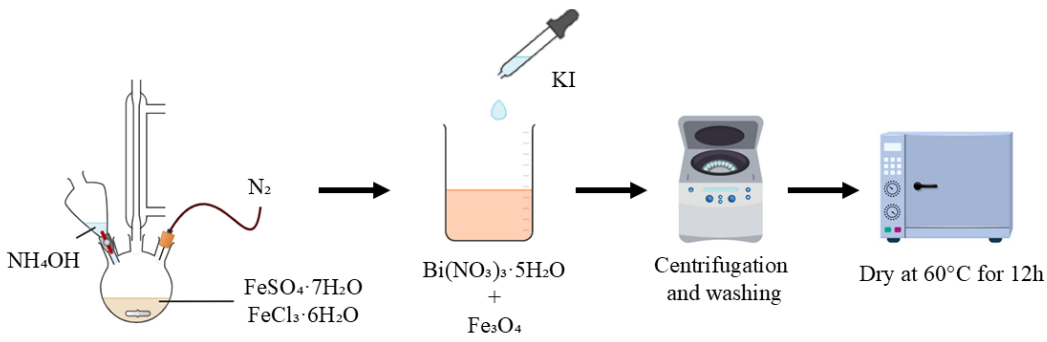


Fig. 1. Schematic illustration of the synthesis of Fe_3O_4/BiOI heterojunction via in-situ precipitation

2.4 Characterization

The crystalline phases and structural properties of BiOI, Fe_3O_4, and Fe_3O_4/BiOI were investigated using X-ray diffraction (XRD) with Cu Kα radiation (λ = 1.5406 Å) and scanning range 10-80°. The surface charge and colloidal stability of BiOI, Fe_3O_4, and Fe_3O_4/BiOI were evaluated by zeta potential and dynamic light scattering (DLS) measurements, from which the zeta potential, Z-average hydrodynamic size, and polydispersity index (PdI) of each sample were obtained. The optical absorption properties of BiOI, Fe_3O_4, and Fe_3O_4/BiOI were investigated using UV–Vis diffuse reflectance spectroscopy (UV–Vis DRS). The corresponding optical band gap energies were estimated from Tauc plots derived from the diffuse reflectance data using the standard Tauc extrapolation method.

2.5 Photocatalytic Performance

The photocatalytic performance of BiOI, Fe_3O_4, and Fe_3O_4/BiOI was evaluated based on the degradation of RhB under visible-light irradiation. A 10 mg/L RhB solution was prepared, and each catalyst was added at a dosage of 1 g/L. H_2O_2 was added at a concentration of 0.1 wt% as an additional oxidant. Before irradiation, the suspension was magnetically stirred in the dark for 15 min to establish adsorption–desorption equilibrium between the catalyst and RhB. The suspension was subsequently irradiated using a 100 W LED lamp as the visible-light source for 60 min. Aliquots were collected at predetermined irradiation times of 0, 15, 30, 45, and 60 min and analysed using UV–Vis spectroscopy to determine the residual RhB concentration. A control experiment containing RhB and the catalyst without H_2O_2 was conducted under otherwise identical dark-equilibration and visible-light irradiation conditions to evaluate the contribution of photocatalytic degradation in the absence of the additional oxidant. The percentage RhB removal and concentration ratio, Ct/Co, were calculated at each irradiation time. The degradation kinetics were evaluated using the pseudo-first-order kinetic model as shown in Eq. 1.

$$\ln(\mathrm{Ct/Co}) = -\mathrm{kt} \quad (1)$$

where Co and Ct are the RhB concentrations at the initial time and at time t respectively, k is the pseudo-first-order rate constant (min^{-1}), and t is the irradiation time (min). The rate constant for each sample was obtained from the slope of the ln(Ct/Co) versus t plot, consistent with the pseudo-first-order approach widely applied to photocatalytic dye degradation studies.

2.6 Phytotoxicity Assessment

The phytotoxicity of the RhB solution before and after photocatalytic treatment was evaluated using a garden cress (*Lepidium sativum*) seed germination bioassay. Garden cress seeds were placed on filter paper in separate Petri dishes and moistened with the untreated RhB solution, photocatalytically treated RhB solution, or tap water as the control. An equivalent volume of each test solution was applied to the filter paper to maintain consistent moisture conditions throughout the experiment. The Petri dishes were maintained under ambient conditions, and seed germination and seedling growth were monitored on Days 1, 3, and 5. The development of the seedlings was assessed by measuring the length at Day 5 periods. The growth response of seedlings exposed to the untreated and treated RhB solutions was compared with that of the tap-water control to evaluate the phytotoxic effects of the dye and the extent of toxicity reduction following photocatalytic

treatment. The results were used to determine whether the photocatalytic process reduced the biological toxicity of the treated solution, in addition to removing RhB from the aqueous phase.

3. Results and Discussion

3.1 Physicochemical Characterization

The crystal structure of BiOI, Fe_3O_4, and the Fe_3O_4/BiOI composite was examined by X-ray diffraction (XRD), as shown in Figure 2. The diffraction pattern of Fe_3O_4 shows peaks at 2θ ≈ 30.2°, 35.6°, 43.2°, 53.5°, 57.1°, and 62.7°, consistent with the (220), (311), (400), (422), (511), and (440) reflections of the cubic inverse spinel structure of magnetite (JCPDS card No. 19-0629) [17], with the (311) reflection as the strongest peak, as expected for Fe_3O_4. The pattern of BiOI shows sharp peaks at 2θ ≈ 9.8° (001), 29.8° (102), 31.8° (110), 37.3° (103), 45.6° (104), 51.5° (114), 55.3° (212), 66.4° (220), and 75.3° (310), matching the tetragonal BiOI structure (JCPDS card No. 10-0445) [18], with the intense (102)/(110) doublet confirming good crystallinity. The pattern of the Fe_3O_4/BiOI composite is dominated by the BiOI reflections at the same positions, together with additional peaks (▲) at 2θ ≈ 35.6°, 43.2°, 57.1°, and 62.7° coinciding with the main reflections of Fe_3O_4, confirming that both crystalline phases coexist in the composite. No peaks attributable to other crystalline impurities were observed. The dominance of the BiOI reflections in the composite pattern is consistent with the zeta-potential, which indicated a BiOI-terminated particle surface.

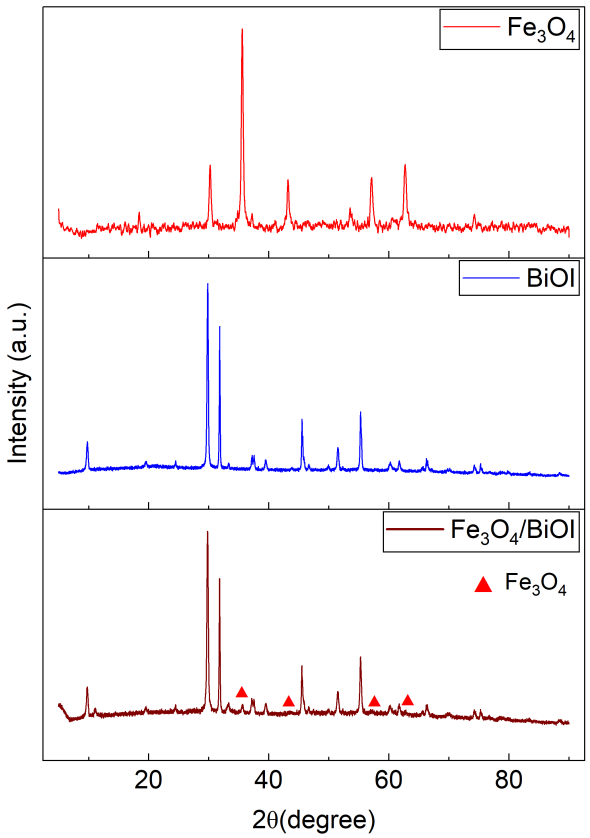


Fig. 2. XRD Patterns of Fe_3O_4, BiOI, and Fe_3O_4/BiOI

The colloidal properties of the individual components and composite were further evaluated using zeta potential, Z-average hydrodynamic size, and polydispersity index (PdI), as summarized in Table 1. BiOI exhibits the most negative zeta potential (-27.6 ± 0.72 mV) and the smallest Z-average particle size (455.4 ± 14.22 nm) of the three samples, consistent with a well-dispersed,

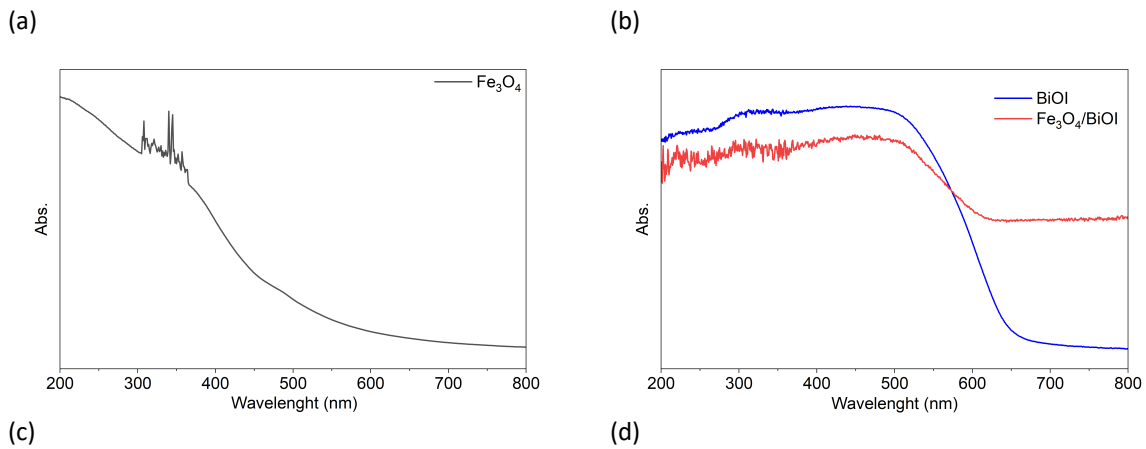
electrostatically stabilised suspension of BiOI nanosheets. Bare Fe_3O_4, in contrast, has a less negative zeta potential (-21.4 ± 1.16 mV), a markedly larger Z-average size (2142.0 ± 425.77 nm), and the highest polydispersity index (PdI = 0.523 ± 0.030), reflecting the well-known tendency of magnetic nanoparticles to agglomerate through magnetic dipole-dipole attraction and weaker electrostatic repulsion [19]. Following in-situ deposition of BiOI, the Fe_3O_4/BiOI composite shows an intermediate zeta potential (-25.3 ± 0.35 mV) that lies closer to that of BiOI, suggesting that the particle surface is predominantly terminated by BiOI. More significantly, the composite's Z-average size (753.8 ± 8.43 nm) is nearly three times smaller than that of bare Fe_3O_4, and its PdI (0.294 ± 0.027) is the lowest of the three samples, compared with 0.523 ± 0.030 for bare Fe_3O_4 and 0.367 ± 0.039 for bare BiOI. This indicates that BiOI deposition disrupts the magnetic agglomeration of Fe_3O_4 and yields a smaller, more uniformly dispersed composite, which is expected to expose a greater accessible surface area for RhB adsorption and photocatalytic reaction, in line with established zeta potential-based colloidal stability trends [20].

Table 1
Zeta Analysis of BiOI, Fe_3O_4, and Fe_3O_4/BiOI

Sample	Zeta Potential (mV)	Z-Average (d.nm)	PdI
BiOI	-27.6 ± 0.72	455.4 ± 14.22	0.367 ± 0.039
Fe_3O_4	-21.4 ± 1.16	2142.0 ± 425.77	0.523 ± 0.030
Fe_3O_4/BiOI	-25.3 ± 0.35	753.8 ± 8.43	0.294 ± 0.027

3.2 Optical Properties

The optical absorption properties of Fe_3O_4, BiOI, and Fe_3O_4/BiOI were investigated using UV-Vis diffuse reflectance spectra and the corresponding Tauc plots obtained using the standard Tauc extrapolation method [21], used to determine the optical band gap of Fe_3O_4, BiOI, and Fe_3O_4/BiOI as shown in Figure 3. The absorption edge of Fe_3O_4/BiOI (Figure 3b) is red-shifted relative to bare BiOI, indicating extended visible light absorption after heterojunction formation. The Tauc plots give a direct band gap of 2.38 eV for Fe_3O_4 (Figure 3c) and indirect band gaps of 1.77 eV for BiOI and 1.08 eV for Fe_3O_4/BiOI (Figure 3d). The pronounced narrowing of the band gap from 1.77 eV in bare BiOI to 1.08 eV in the composite indicates strong electronic coupling between Fe_3O_4 and BiOI at the heterojunction interface, consistent with the red-shifted absorption edge and with trends reported for other BiOI-based heterojunctions [9]. This narrowed band gap allows Fe_3O_4/BiOI to harvest a larger portion of the visible spectrum and generate photoexcited charge carriers more readily, consistent with the substantially higher RhB removal and rate constant of Fe_3O_4/BiOI reported in Figure 4.



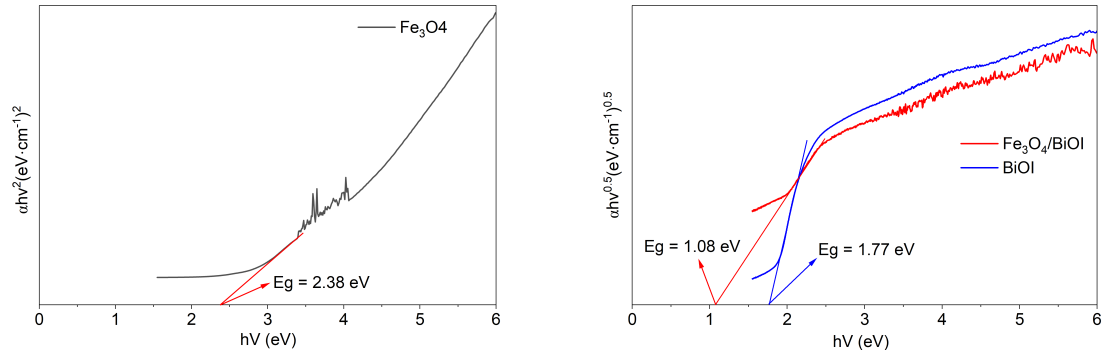
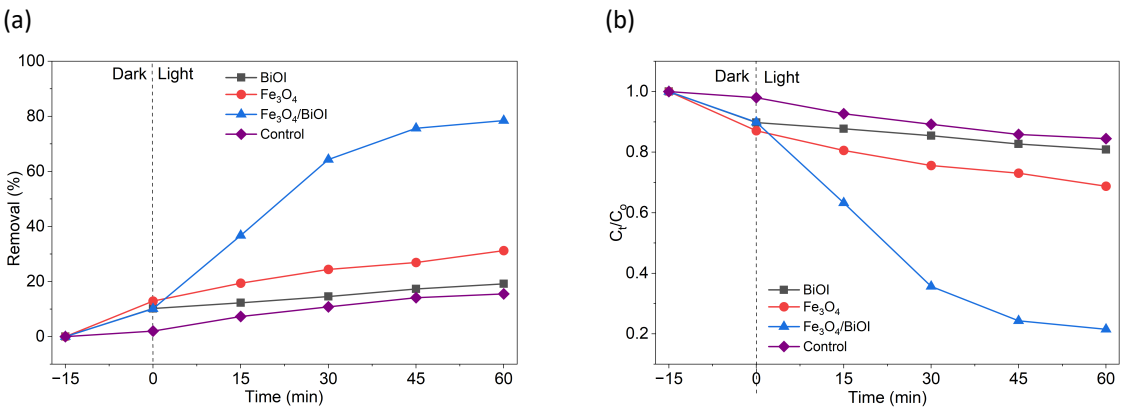


Fig. 3. UV-Vis DRS of Fe_3O_4 (a), BiOI and Fe_3O_4/BiOI (b), and The Corresponding Tauc Plots for Band Gap Estimation of Fe_3O_4 (c), BiOI and Fe_3O_4/BiOI (d)

3.3 Photocatalytic Performance

The photocatalytic activity of Fe_3O_4, BiOI, and Fe_3O_4/BiOI was evaluated using RhB as the model pollutant under visible-light irradiation. Figure 4a shows the RhB removal profile over a 15-minute dark adsorption-equilibrium period followed by 60 minutes of visible light irradiation. Fe_3O_4/BiOI removed approximately 79% of RhB within 60 minutes, compared with only 31% for Fe_3O_4 and 20% for BiOI alone. A control experiment (RhB and catalyst under visible light without H_2O_2) removed only approximately 15–16% of RhB over the same period, corresponding to a Ct/Co of about 0.84 and closely comparable to bare BiOI, confirming that direct photolysis contributes only marginally to RhB removal in the absence of a catalyst. The corresponding Ct/Co decay curves (Figure 4b) show the same trend in reverse, with the composite reaching Ct/Co of about 0.22 while BiOI and Fe_3O_4 remained above 0.80 and 0.68 respectively. The degradation data fit the pseudo-first-order model well (Figure 4c), and the derived rate constants (Figure 4d) confirm the trend quantitatively: k = 0.00255 min^{-1} for BiOI, 0.00469 min^{-1} for Fe_3O_4, and 0.02319 min^{-1} for Fe_3O_4/BiOI, representing enhancements of approximately 9.1-fold and 4.9-fold over BiOI and Fe_3O_4 respectively, a magnitude of enhancement comparable to that reported for other visible-light-active nanocomposite photocatalysts. This marked improvement is attributable to the heterojunction formed between Fe_3O_4 and BiOI, which promotes separation of photogenerated electron-hole pairs and suppresses recombination, in agreement with recent reports on magnetically coupled bismuth oxyhalide photocatalysts [11], [12]. The smaller, more uniform particle size of the composite noted in Table 1 is also likely to contribute, since reduced agglomeration increases the surface area available for radical generation.



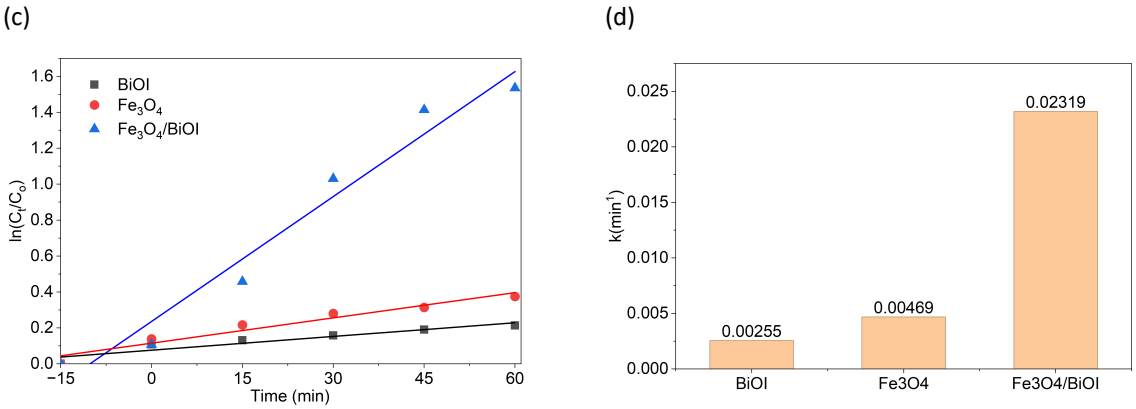
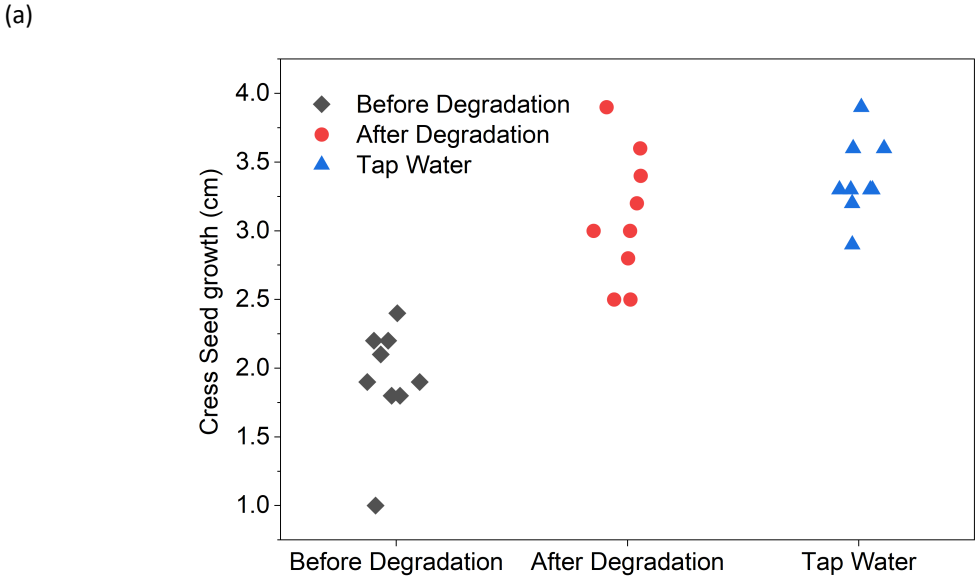


Fig. 4. Removal Percentage of Rhodamine B dye (a), Ct/Co (b), First-Order Kinetic (c), and Kinetics of Dye Removal for Fe_3O_4, BiOI, and Fe_3O_4/BiOI (d), with a photolysis-only Control (RhB + light, no catalyst/H_2O_2) shown in (a) and (b)

3.4 Phytotoxicity Performance

The potential reduction in toxicity following photocatalytic treatment was evaluated using garden cress (Lepidium sativum) as a biological indicator. Figure 5 compares seedling growth following exposure to untreated RhB solution, photocatalytically treated RhB solution, and tap water as the control. Figure 5a shows that garden cress grown in the untreated RhB solution (before degradation) reached only 1.0 to 2.4 cm, markedly stunted relative to the tap water control (2.9 to 3.9 cm), confirming that the dye solution was phytotoxic, consistent with reports of RhB ecotoxicity [1] and with the known sensitivity of Lepidium sativum to pollutant stress [22]. Following photocatalytic treatment with Fe_3O_4/BiOI, seedling growth recovered to 2.5 to 3.9 cm, a range that overlaps closely with the tap water control. This is an important result because photocatalytic intermediates can occasionally be more toxic than the parent dye if degradation is incomplete. The recovery of growth close to the control level indicates that the treatment genuinely detoxified the solution rather than simply decolourising it, in line with recent phytotoxicity assessments of photocatalytically treated dye effluents [15], [23]. The photographic record in Figure 5b and 5c across Day 1, Day 3, and Day 5 visually corroborates this quantitative recovery.



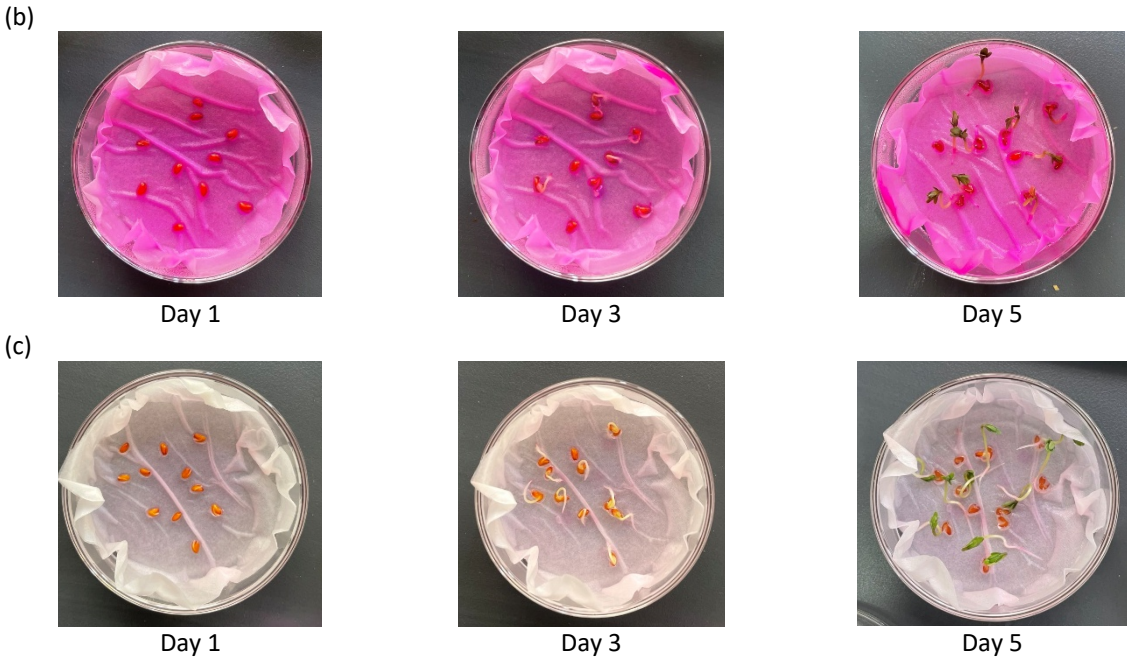


Fig. 5. Toxicity Test on Garden Cress Growth (a), Garden Cress Growth Observation Before Degradation (b), and After Degradation (c) from Day 1 to Day 5

4. Conclusions

A magnetically recoverable Fe_3O_4/BiOI heterojunction photocatalyst was successfully synthesised via a facile in-situ precipitation route. Zeta potential and dynamic light scattering analysis showed that in-situ BiOI deposition reduces the magnetic agglomeration characteristic of bare Fe_3O_4, producing a smaller and more uniformly dispersed composite. UV-Vis diffuse reflectance analysis further showed that the band gap narrowed from 1.77 eV for BiOI to 1.08 eV for Fe_3O_4/BiOI, confirming stronger visible light harvesting and more efficient interfacial charge transfer after heterojunction formation. Under visible light, Fe_3O_4/BiOI removed approximately 79% of Rhodamine B within 60 minutes, following pseudo-first-order kinetics with a rate constant 4.9 to 9.1 times higher than that of Fe_3O_4 or BiOI alone, an enhancement attributed to this narrowed band gap and to more efficient charge separation at the Fe_3O_4/BiOI interface. A garden cress germination bioassay confirmed that this improved degradation translated into genuine detoxification, with seedling growth in the treated solution recovering close to the tap water control. Together with the practical advantage of magnetic recoverability, these results support Fe_3O_4/BiOI as a promising, reusable photocatalyst for the visible-light-driven remediation of dye-contaminated water. Future work should identify the dominant reactive species through radical scavenging experiments and test performance in real textile wastewater.

Acknowledgement

This study was funded through an industry–university collaboration between EMZI Holdings Sdn. Bhd. and Universiti Teknologi MARA (UiTM) under research grant no (MIH-(008/2020)).

References

[1] Md. M. Islam, A. R. Aidid, J. N. Mohshin, H. Mondal, S. Ganguli, and A. K. Chakraborty, "A Critical Review on Textile Dye-Containing Wastewater: Ecotoxicity, Health Risks, and Remediation Strategies for Environmental Safety," *Cleaner Chemical Engineering* 11 (2025): 100165. https://doi.org/10.1016/j.clce.2025.100165.

[2] P. S. Priya, P. Pratiksha Nandhini, S. Vaishnavi, V. Pavithra, M. H. Almutairi, B. O. Almutairi, S. Arokiyaraj, R. Pachaiappan, and J. Arockiaraj, "Rhodamine B, an Organic Environmental Pollutant Induces Reproductive Toxicity in Parental and Teratogenicity in F1 Generation In Vivo," *Comparative Biochemistry and Physiology Part C: Toxicology & Pharmacology* 280 (2024): 109898. https://doi.org/10.1016/j.cbpc.2024.109898.

[3] Aayushi and S. Pandey, "From Conventional Treatment to Light-Driven Remediation: A Review of Strategies for Treatment of Dye-Contaminated Wastewater," *Frontiers in Environmental Engineering* 5 (2026). https://doi.org/10.3389/fenve.2026.1847347.

[4] D. Ramutshatsha-Makhwedzha and A. Munyengabe, "Catalytic Materials Applied for Dye Removal in Advanced Oxidation Processes: A Mini Review of Studies from 2015 to 2025," *Discover Water* 6, no. 1 (2026): 27. https://doi.org/10.1007/s43832-026-00342-1.

[5] J. Liu, J. Shi, and H. Deng, "Current Status of Research on BiOX-Based Heterojunction Photocatalytic Systems: Synthesis Methods, Photocatalytic Applications and Prospects," *Journal of Environmental Chemical Engineering* 11, no. 5 (2023): 110311. https://doi.org/10.1016/j.jece.2023.110311.

[6] B. Benalioua, I. Benyamina, M. Mansour, K. Mensri, A. Bentouami, and B. Boury, "Synthesis of a New Multi-Heterojunction Photocatalyst BiOI/Bi2O3/MgO and Its Photocatalytic Efficiency in the Degradation of Rhodamine B under Visible Light," *Desalination and Water Treatment* 281 (2023): 265–275. https://doi.org/10.5004/dwt.2023.29144.

[7] B. Wang, L. Huang, S. Li, and L. Qi, "Synthesis of Co3O4/BiOBr/BiOI Ternary Heterostructure and Its Photocatalytic Degradation of RhB," *Water, Air, & Soil Pollution* 235, no. 7 (2024): 406. https://doi.org/10.1007/s11270-024-07192-4.

[8] O. Ogbeifun, S. M. Tichapondwa, and E. M. N. Chirwa, "Degradation of Rhodamine B Dye on BiOIO3/Bi12O17Cl2 Heterostructure Photocatalyst under Visible Light Activation," *South African Journal of Chemical Engineering* 54 (2025): 63–69. https://doi.org/10.1016/j.sajce.2025.07.005.

[9] S. Yang, T. Wu, K. Li, P. Huang, W. Li, Y. Zhuo, K. Liu, Z. Yang, and D. Han, "Photocatalytic Enhancement and Recyclability in Visible-Light-Responsive 2D/2D g-C3N4/BiOI p-n Heterojunctions via a Z-Scheme Charge Transfer Mechanism," *Molecules* 29, no. 22 (2024): 5418. https://doi.org/10.3390/molecules29225418.

[10] X. Li, L. Du, Z. Wan, D. Xu, and C. Liu, "A Novel n-p-n Type ZnO/BiOI/AgI Ternary Heterojunction with Enhanced Visible-Light Photocatalytic Performance for Pollutant Degradation and Antibacterial Applications," *Materials Advances* (2025). https://doi.org/10.1039/d5ma00354g.

[11] S. Nonthing, A. Panchakeaw, R. Dulyasucharit, H. Nakajima, and S. Nanan, "Fe3O4/BiOCl Photocatalyst with Magnetic Recovery Property for Solar-Light-Responsive Removal of Rhodamine B Dye," *OpenNano* 26 (2025): 100260. https://doi.org/10.1016/j.onano.2025.100260.

[12] N. Madima, K. K. Kefeni, S. B. Mishra, A. K. Mishra, and A. T. Kuvarega, "Fabrication of Magnetic Recoverable Fe3O4/TiO2 Heterostructure for Photocatalytic Degradation of Rhodamine B Dye," *Inorganic Chemistry Communications* 145 (2022): 109966. https://doi.org/10.1016/j.inoche.2022.109966.

[13] T. B. Mbuyazi and P. A. Ajibade, "Photocatalytic Degradation of Organic Dyes by Magnetite Nanoparticles Prepared by Co-Precipitation," *International Journal of Molecular Sciences* 25, no. 14 (2024): 7876. https://doi.org/10.3390/ijms25147876.

[14] M. A. M. Castro, R. A. Oliveira, J. M. P. Silva, M. D. Teodoro, U. C. Silva, M. R. D. Bomio, and F. V. Motta, "Solar-Enhanced Photodegradation of Dye and Drug Mixture and Evaluation of Phytotoxicity on Seed Germination and Growth by an Eggshell HAp/Nb2O5 Heterostructure," *Ceramics International* 50, no. 11 (2024): 19124–19136. https://doi.org/10.1016/j.ceramint.2024.03.011.

[15] M. Varshini, K. Ravichandran, M. Ayyanar, R. Anandhi, and R. Manimekalai, "Effective Dye Detoxification by *Cassia fistula* Flower Extract-Powered Photocatalytic Nanocomposite, SnO2/rGO and Phytotoxicity Evaluation of Treated Water Using Cowpea Seeds," *Journal of Environmental Chemical Engineering* 12, no. 5 (2024): 113270. https://doi.org/10.1016/j.jece.2024.113270.

[16] M. M. Ba-Abbad, A. Benamour, D. Ewis, A. W. Mohammad, and E. Mahmoudi, "Synthesis of Fe3O4 Nanoparticles with Different Shapes through a Co-Precipitation Method and Their Application," *JOM* 74, no. 9 (2022): 3531–3539. https://doi.org/10.1007/s11837-022-05380-3.

[17] E. A. Namikuchi, R. D. L. Gaspar, D. S. da Silva, I. M. Raimundo Jr., and I. O. Mazali, "PEG Size Effect and Its Interaction with Fe3O4 Nanoparticles Synthesized by Solvothermal Method: Morphology and Effect of pH on the Stability," *Nano Express* 2, no. 2 (2021): 020022. https://doi.org/10.1088/2632-959X/ac0596.

[18] S. Rahdar, M. Davoudi, N. E. Hassan, S. Fathi-Karkan, F. Barjasteh Askari, M. Shams, and A. A. Mohammadi, "Amine Functionalized Reduced Graphene Oxide Decorated with BiOI and Ag3PO4 as a Novel Visible Light Catalyst against RhB," *Scientific Reports* 15 (2025): 37649. https://doi.org/10.1038/s41598-025-21474-9.

[19] J. Rodriguez-Loya, M. Lerma, and J. L. Gardea-Torresdey, "Dynamic Light Scattering and Its Application to Control Nanoparticle Aggregation in Colloidal Systems: A Review," *Micromachines* 15, no. 1 (2024): 24. https://doi.org/10.3390/mi15010024.

[20] D. J. Pochapski, C. Carvalho dos Santos, G. W. Leite, S. H. Pulcinelli, and C. V. Santilli, "Zeta Potential and Colloidal Stability Predictions for Inorganic Nanoparticle Dispersions: Effects of Experimental Conditions and Electrokinetic Models on the Interpretation of Results," *Langmuir* 37, no. 45 (2021): 13379–13389. https://doi.org/10.1021/acs.langmuir.1c02056.

[21] E. S. Welter, S. Garg, R. Gläser, and M. Goepel, "Methodological Investigation of the Band Gap Determination of Solid Semiconductors via UV/Vis Spectroscopy," *ChemPhotoChem* 7, no. 6 (2023). https://doi.org/10.1002/cptc.202300001.

[22] V. M. Schulz, C. Scherr, S. Baumgartner, and A. Tournier, "A Versatile *Lepidium sativum* Bioassay for Use in Ecotoxicological Studies," *Scientific Reports* 15, no. 1 (2025). https://doi.org/10.1038/s41598-025-17215-7.

[23] A. Sudha, I. Manimehan, R. Shalini, M. Varshini, K. Ravichandran, M. Ayyanar, P. K. Praseetha, and D. Saravanakkumar, "Assessment of De-Toxicity of Treated Dye Solution via Seed Germination Test: Photocatalytic Treatment by *Morinda citrifolia* Leaf Extract Mediated ZnO/g-C3N4 Nanocomposite," *Materials Science in Semiconductor Processing* 178 (2024): 108437. https://doi.org/10.1016/j.mssp.2024.108437.

[24] N. L. S. Mustapa, N. F. A. Bakar, A. H. Nordin, et al., "Band-Engineered Heterostructure Photocatalytic Micromotors for Autonomous Water Remediation," *Discover Chemical Engineering* (2026). https://doi.org/10.1007/s43938-026-00147-7.